Landslide Susceptibility Mapping and Risk in the Tamzoura Municipality, Algeria

Freddy Marten

1 Introduction

Tamzoura, in the Aïn Témouchent province of Algeria, is a remote municipality with relatively little infrastructure. According to OpenStreetMap contributors (2024) it covers 231 km^2 and around 9500 people likely live there (OpenStreetMap contributors 2024; Aïn Témouchent Government 2010). Given that availability of data on the villages and hamlets in the region is poor, I expect this to have grown since then. Residents are mostly situated in Tamzoura itself. This makes it the main area of concern when it comes to landslides, alongside infrastructure and other settlements nearby. With no railways in the region, the primary infrastructure is a road network, notably the major N108 road a limited canal network (OpenStreetMap contributors 2024).

As shown in Figure 1, Tamzoura is in northwest Algeria not far from the Meditteranean Sea, bordered to the north by the Sebkha d'Oran salt lake (ibid.). Figure 1 also shows the extreme difference in land cover on the northern and southern sides of a fault line that splits Tamzoura in two. Far-south and north of this fault line, there is not much infrastructure and very few settlements. But just north of the fault line, where the N108 lies, is the most developed part of Tamzoura - perhaps because of the road itself. Most land north of the fault line is used for agriculture, whereas in the south, land is largely uninhabited.

Bounemeur et al. (2022) underline the dangerous combination of uncontrolled development of urban areas in landslide-prone regions. In the Asia-Pacific, regions most vulnerable to landslides are reportedly the least developed (Kjekstad and Highland 2009, p. 584). Of key interest in this report is whether the Tamzoura region is at a similar risk. This stresses the importance of landslide susceptibility analysis in areas such as Tamzoura. If it is demonstrated to be susceptible this would make it more vulnerable. Therefore, by informing civilians and authorities in the region, the negative effects from a potential landslide can be mitigated.

The United States Geological Survey uses 'the movement of rock, earth or debris down a slope' as their definition of landslides. Crucially, different types of materials might move down slopes under very different circumstances. I avoiding converting variables to binary where possible in this report to account for these different types of landslides. Yalcin (2007) highlights that heavy rainfall events are the typical cause of severe landslides. Kjekstad and Highland (2009, p. 576) shows the steep economic costs of landslides in different nations.

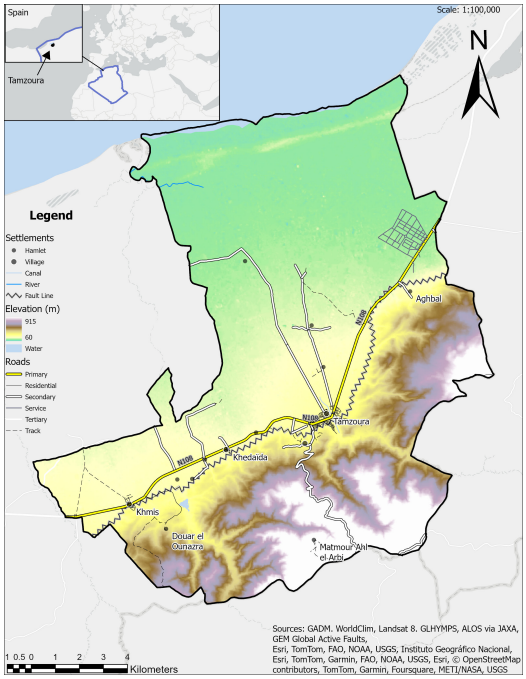

Figure 1: Context on Tamzoura with location, infrastructure, and elevation.

2 Methodology

2.1 Overview

I pre-processed all nine datasets displayed in Figure 2, setting them to a uniform coordination system. Here, this was the *World Geodetic System 1984 Complex Universal Transverse Mercator, Zone 30N*. I geo-processed and analysed each dataset iteratively; geo-processing informed my analysis and vice-versa (Figure 2). Techniques key to this report include raster calculation, reclassification and fuzzy membership. I will first provide more detail on the geo-processing and analysis of the layers used - and why some were omitted - detailing thresholds and weightings explicitly. I then explain the methodology behind the two scenarios landslide susceptibility maps (LSMs) themselves. After showing these results I discuss their value and what they mean for future research, before using them to reach a final verdict on landslide susceptibility in Tamzoura.

2.2 Precipitation

As discussed earlier, the greatest cause of landslides historically is precipitation. Heavy rainfall events are often the first domino to fall, which ultimately cause landslides (Ahmed 2015, p. 1077). I used 1km resolution precipitation data via Fick and Hijmans (2017) that measures precipitation in mm. This resolution is much lower than some of the other datasets I used, and for the LSM to be at a useful resolution I used bilinear resampling with a 10m resolution to generalise this precipitation data at an increased resolution. I show this in Figure 3 which shows the transition from blocky, 1km resolution data to a more continuous gradient. The smoothed layer, of course, shows the trend more clearly, with higher rainfall found southeast of the fault line. Considered alongside basic theory on the build-up of rain clouds in higher elevation terrain and the slope in Figure 9, the right-hand-side of Figure 3 seemed very reasonable and may have the added benefit of removing some Guassian noise. The smoothed map in Figure 3 is less true to reality, but essential to produce useful LSMs.

2.3 Soil Permeability

A logical next step from rainfall is assessing how much rain permeates the surface of Tamzoura. For this I used Gleeson (2018), a selection of polygons representing soil permeability in different regions of Tamzoura. According to Gleeson et al. (2011) permeability measures 'the ease of fluid flow through porous rocks and soils'. The study area had only three different levels of permeability: -15.2, -13 and -11.8. These are really the geometric means of the base-10 logarithmic permeability, denoted k' in equation 1, where individual permeability measurements are k_i (ibid.).

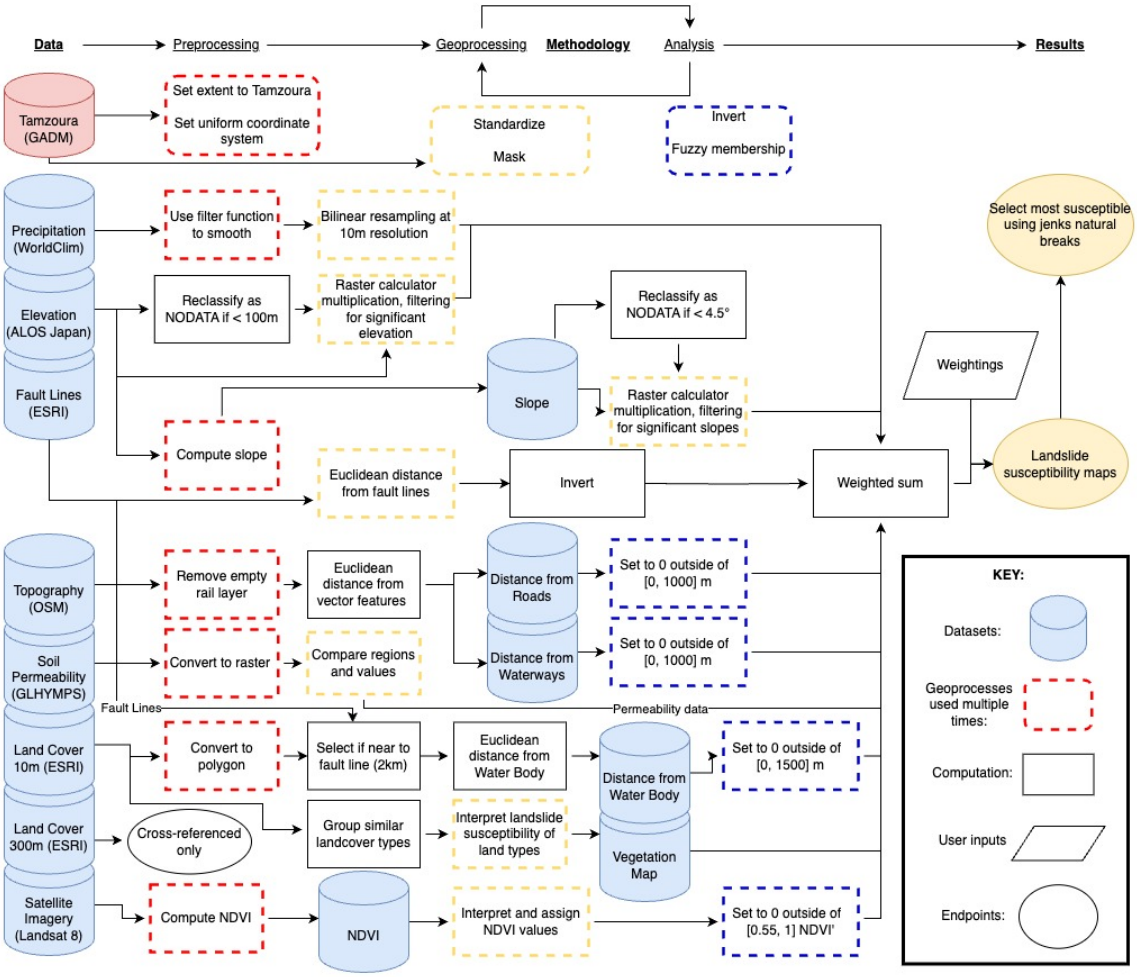

Figure 2: Flowchart showing methodology

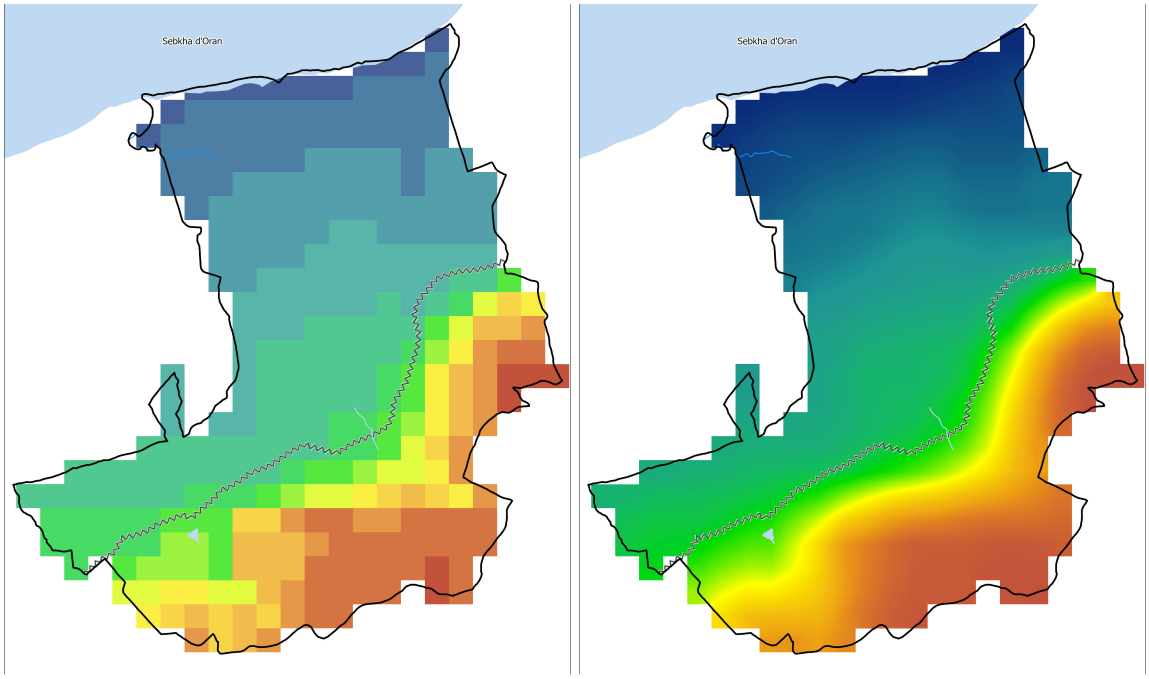

Figure 3: Precipitation layer from 1km resolution layer (left) to smoothed layer following bilinear resampling (right).

$$k' = \left(\prod_{i=1}^{n} \log(k_i) \right)^{1/n} \quad (1)$$

Gleeson et al. (2011) highlight that this transformation is useful as raw permeability k varies over 13 orders of magnitude. They demonstrate this clearly in Gleeson et al. (Figure 1, 2011) and Freeze and Cherry (1979). In Tamzoura, the region to the north of the fault line k' is all valued at -13. This corresponds to unconsolidated material (or colluvium) (Gleeson et al. 2011). Soralump et al. (2021) confirms the basic theory stating that colluvium deposits lack stability and have a tendency for 'recurrent downward movement'.

2.4 Elevation and Slope

To check whether such movement is possible, I incorporated a measure of slope. I computed such a layer using elevation data, specifically the Precise Global Digital 3D Map from the Advanced Land Observing Satellite (ALOS) and the Japan Aerospace Exploration Agency (JAXA). This layer's elevation statistics are accurate within 5m of altitude with a 30m resolution Tadono et al. (2016). This elevation data itself is also useful, for example because a steep slope only 5m high is not of much concern. Generally, the higher the elevation, the more susceptible a region is to a landslide.

To converted this into a slope I used ArcGIS Pro's slope feature. Highland and Bobrowsky (n.d., Section 1, 29) acknowledge that sometimes landslides occur with a slope as little as 1 or 2°. So, I reclassified the slope as NODATA if the slope was shallow (le to 2°) to avoid considering any areas where the land has nowhere to slide. Leaving a 1-2° slope within the overlay allowed too many options, reducing the interpretability of the LSMs. With a threshold of 4.5°, only the region south of

the fault line was considered susceptible. I also standardised the data by dividing all slope values by the maximum slope, 54.8°. I show this in Equation 2, where Z is a vector of elevation values associated with every 30x30m location. Unless otherwise stated this formula will be used to standardize all variables.

$$Z' = \frac{Z}{\max\{Z\}} \tag{2}$$

Multiplying the reclassified layer by the standardised one removes the areas of Tamzoura with a slope $< 2°$. It does not however, simplify the layer to take binary values .

For elevation a very similar process was used. Instead I standardised using the maximum elevation, 942m and reclassified the layer as NODATA when the elevation was $\leq$ 100m (ELEV classified as NODATA). The latter choice is quite natural when considering 1, which shows that there is consistently low relative elevation, (between 60 and 190m), north of the fault line. The average elevation in Tamzoura is 237m, and minimum 60m.

2.5 NDVI and Land cover

There were many options for incorporating land cover into LSMs. The 300m map was not suitable for an LSM because the resolution was too low to detect patches of bare ground that potentially prone to a landslide if they lie next to a large enough woodland. Worse still, it had significant contradictions with the high-resolution imagery basemap and 10m resolution ESRI map.

The Landsat 8 hyperspectral image usefully had almost no cloud cover. However, graphs of band values across the map hinted towards difficulty differentiating land cover in Tamzoura. I attempted to derive a landcover map from it with a supervised approach regardless - using the 10m land cover map or imagery basemap to verify. It struggled to differentiate all land cover types, except crops - which NDVI better identifies anyway. The stark difference in land cover between the north and south of the fault line was not detected. This ruled out a landsat-derived land cover map.

Accordingly, I used the 10m land cover map, which seems a much more appropriate resolution for the analysis. Similar land cover types were grouped together. In order of increasing vegetation: grassland and bareground were treated the same, as were water and herbaceous wetland and cropland and shrubland. This produced a vegetation map shown in Figure 7 (appendix). These groups were then assigned values between 0 and 1 with bare ground and grass at 1 and trees at 0.

Normalised Difference Vegetation Index (NDVI) was calculated using bands from the Landsat 8 image. NDVI is defined by equation 3, a function of the near infrared (NIR) and red bands of this hyperspectral image.

$$\text{NDVI} := \frac{\text{NIR} - \text{RED}}{\text{NIR} + \text{RED}}. \tag{3}$$

Kshetri (2018) provide a useful guide to using NDVI stating that it takes values between -1 and 1, where negative values represent water bodies (or clouds), values between -0.1 and and 0.1 barren areas, and values closer to 1 dense areas of vegetation. Since NDVI takes values between -1 and 1, I used Equation 4 to standardise to a $[0, 1]$ scale.

$$\text{NDVI}' = \frac{1 + \text{NDVI}}{2}. \tag{4}$$

2.6 Vector Data

I also consider Vector data describing roads, settlements and waterways in Tamzoura - and the

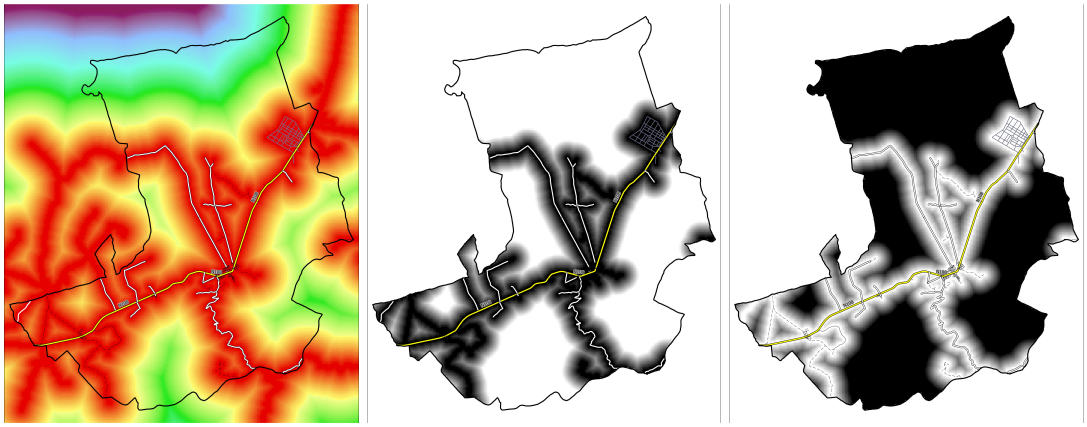

Figure 4: Process for creating a distance from roads layer using fuzzy membership. Distance from roads is calculated (left) then compute fuzzy membership (middle) and finally invert (right).

1km surrounding area. As shown in Figure 4 for roads, I first compute a layer describing the Euclidean distance (see Equation 6) from this vector data, then apply fuzzy membership before inverting the variables using the raster calculator as in Equation 5.

$$\mathrm{X}_{\mathrm{Inv}} = |X - \max\{X\}|. \tag{5}$$

I did the same for water bodies but, due to a discrepancy between the 10m land cover data and the OpenStreetMap (OSM) water bodies data, I converted the singular water body identified within Tamzoura's borders and extracted it as a polygon - using its proximity to the fault line - within 2km - to select it. I opted not to include Sebkha d'Oran in either LSM because as previously shown there is little elevation, slope or rainfall in this region.

$$d_{\mathrm{Eucl}}(x, y) = \sqrt{(x - y)^2}. \tag{6}$$

2.7 Weighted Overlay

I chose the weighted overlay approach because only slope and elevation had some strict effect on landslide susceptibility that allowed whole regions to be ruled out. Most variables seem to have continuous relationships with landslide susceptibility. The trade-off here is that a weighted overlay map might be less interpretable. However, processing of these results gives an interpretable map without unsubstantiated assumptions. I used two weighting schemes - one with all the variables included, *All Effects*, and another with only the main effects, *Main Effects*. Given the region's low population, roads might receive little use and a very low chance of causing a landslide. Some of the layers have greater uncertainty than others. Therefore, I excluded them as shown in the *Main Effects* column of Table 1. I gave precipitation, the fault line, slope and soil permeability the highest weightings in both settings because these effects will likely have a high impact regardless of unknown data - such as how many trees have been felled or how busy the region is. Further, precipitation is highly linked to soil permeability and slope to elevation. Not using them in pairs is only really using half a variable.

I used Jenks (1967) Natural Breaks algorithm to split the susceptibility map into three classes. This technique is similar to k-means clustering (Stein-

Layer	All Effects	Main Effects
Ndvi	0.10	0.00
Slope	0.20	0.25
Waterbody	0.05	0.00
Waterway	0.05	0.00
Roads	0.05	0.00
Fault	0.15	0.25
Vegetation	0.05	0.00
Permeability	0.10	0.20
Elevation	0.05	0.05
Precipitation	0.20	0.25
Sum	1.00	1.00

Table 1: Weights for Landslide Susceptibility Scenarios

Susceptiblity	All Effects	Main Effects
Lower	0.61	0.65
Medium	0.67	0.72
Higher	0.81	0.88

Table 2: Landslide Susceptiblity break points using Jenks Natural Breaks

haus et al. 1956; MacQueen et al. 1967) with one-dimensional data. First, the mean of the variable is calculated, then, the sum of the squared differences between each value in the variable and the mean (Equation 7).

$$\text{SSD} = \sum_{i=1}^{n} (x_i - \bar{x})^2 \tag{7}$$

In the second part of the algorithm, the same idea is repeated but now for every sequential subset of values. The thresholds causing the subsets to have the lowest SSD are the natural breaks. Shown in Table 2, are the three groupings calculated for each scenario. I finally separated the most susceptible regions in each scenario.

3 Results

Figures 8 and 10 show two relatively similar LSMs with some key, albeit subtle differences. Figure 5 includes regions closer to roads and infrastructure than Figure 6, mainly along the major N108 road

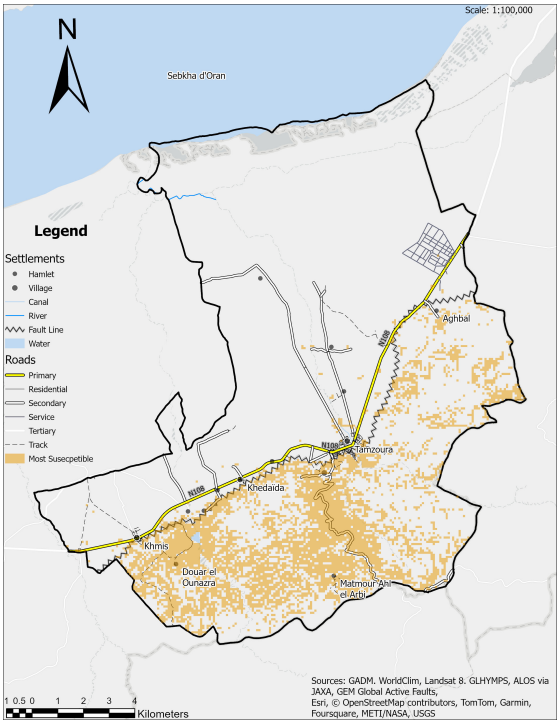

Figure 5: Landslide susceptibility map with all effects included: higher susceptibility only

and near Tamzoura village itself. Both maps show that the most susceptible regions are predominantly south of the fault line, and more strongly south and southwest of Tamzoura.

First, I consider, Figure 5, the scenario with all effects. With infrastructure, the road running south from Tamzoura village is among the areas of highest risk, followed by most of the roads that cross the fault line. Tamzoura village's short canal system is also at risk. Settlements in southern regions of Tamzoura are very close to susceptible regions but appear as though they could be safer. The unnamed village just south of Tamzoura seems particularly at risk aswell as Matmour Ahl el Arbi and Douar el Ounazra. In Figure 6, these settlements are, as expected, not at such a risk because the effects of roads are not accounted for. I saw this combination of two LSMs would be more practical for authorities who will know which represents Tamzoura best. If Tamzoura has grown

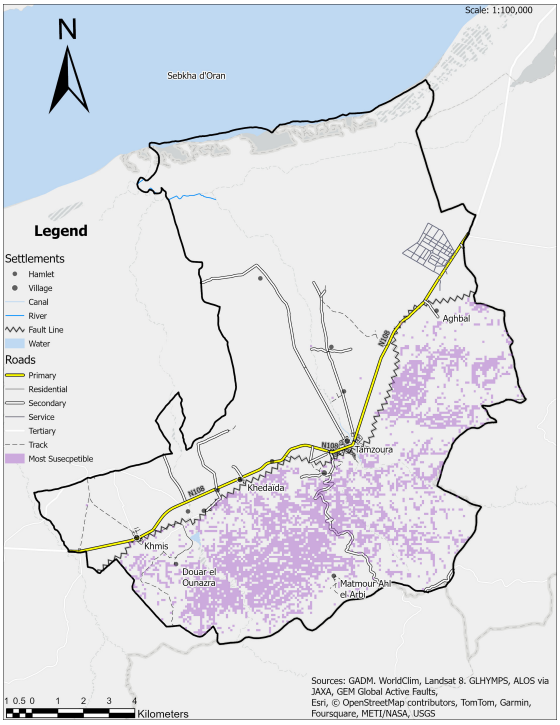

Figure 6: Landslide susceptibility map with main effects included: higher susceptibility only

rapidly since 2010, and has a much larger population now than around 9500, Figure 5 is better. If Tamzoura has not changed, or changed in such a way that roads are not used particularly often, the main effects LSM in Figure 6 might be better. By using two LSMs, maximum uncertainty in the available data is accounted for, at least without missing out vital factors, and assumptions about the data are relaxed to make the findings as useful as possible.

4 Discussion and Conclusion

Our LSMs, whilst showing the parts of Tamzoura most susceptible to landslides, do not say whether a landslide is likely or not. I looked for some historical landslide data to accomplish this but could not find any recorded instances. Even if there has no recent landslides in Tamzoura, studying multiple similar regions simultaneously in future research might provide a better measure of the likelihood of landslides in regions within a given period. The methodology used in this report, could be easily scaled up to include additional municipalities and add historical data into the mix. This would allow us to build a stronger supervised version of the model I have produced. In addition, the 30m resolution of these LSMs stems from the elevation and slope data underpinning them. Substituting in higher resolution data could create more comprehensive LSMs.

So in conclusion, with this fuzzy weighted sum approach I have identified regions in Tamzoura which seem most at susceptible to landslides. This is not to say that these regions are likely to have landslides - only that, based on the methodology producing this report - they seem more susceptible than other parts of Tamzoura. The powerful result that the N108 major road through Tamzoura is not the most susceptible part of the region is somewhat reassuring, since this probably has the most traffic in the region. Again, data on road use in Tamzoura might enhance the results - much like how soil permeability combined with precipitation data gives a measure of how sensitive land is to rainfall. This data does not have to be digital - this might not exist; ground observations or conversation with residents would better inform future landslide susceptibility analysis there. Despite these limitations, the LSMs in this report provide a guide to the minor roads and settlements at risk of landslides in Tamzoura.

[**2500 Words**]

References

Ahmed, Bayes (2015). "Landslide susceptibility mapping using multi-criteria evaluation

techniques in Chittagong Metropolitan Area, Bangladesh". In: *Landslides* 12.6, pp. 1077–1095. DOI: 10.1007/s10346-014-0521-x. URL: https://doi.org/10.1007/s10346-014-0521-x.

Aïn Témouchent Government (2010). *DISTRIBUTION OF THE TOTAL RESIDENT POPULATION AND AVERAGE DENSITY BY MUNICIPALITY (Estimate Year 2010) — web.archive.org*. https://web.archive.org/web/20110310063229/http://www.wilaya-aintemouchent.dz:80/DPAT/francais/raparation.html. [Accessed 14-05-2024].

Bounemeur, Nadira et al. (2022). "Landslides in Mila town (northeast Algeria): causes and consequences". In: *Arabian Journal of Geosciences* 15.8, p. 753.

Fick, Stephen E. and Robert J. Hijmans (2017). "WorldClim 2: new 1-km spatial resolution climate surfaces for global land areas". In: *International Journal of Climatology* 37.12, pp. 4302–4315. DOI: https://doi.org/10.1002/joc.5086. eprint: https://rmets.onlinelibrary.wiley.com/doi/pdf/10.1002/joc.5086. URL: https://rmets.onlinelibrary.wiley.com/doi/abs/10.1002/joc.5086.

Freeze, R. Allan. and John A. Cherry (1979). *Groundwater*. eng. Englewood Cliffs, N.J.

Gleeson, Tom (2018). *GLobal HYdrogeology MaPS (GLHYMPS) of permeability and porosity*. Version V1. DOI: 10.5683/SP2/DLGXYO. URL: https://doi.org/10.5683/SP2/DLGXYO.

Gleeson, Tom et al. (2011). "Mapping permeability over the surface of the Earth". In: *Geophysical Research Letters* 38.2. DOI: https://doi.org/10.1029/2010GL045565. eprint: https://agupubs.onlinelibrary.wiley.com/doi/pdf/10.1029/2010GL045565. URL: https://agupubs.onlinelibrary.wiley.com/doi/abs/10.1029/2010GL045565.

Highland, Lynn and Peter Bobrowsky (n.d.). "The Landslide Handbook—a Guide to Understanding Landslides: A Landmark Publication for Landslide Education and Preparedness". In: pp. 75–85. ISBN: 978-3-642-22086-9. DOI: 10.1007/978-3-642-22087-6-5.

Jenks, George F. (1967). "The Data Model Concept in Statistical Mapping". In: URL: https://api.semanticscholar.org/CorpusID:215850874.

Kjekstad, Oddvar and Lynn Highland (2009). "Economic and Social Impacts of Landslides". In: *Landslides – Disaster Risk Reduction*. Ed. by Kyoji Sassa and Paolo Canuti. Berlin, Heidelberg: Springer Berlin Heidelberg, pp. 573–587. ISBN: 978-3-540-69970-5. DOI: 10.1007/978-3-540-69970-5_30. URL: https://doi.org/10.1007/978-3-540-69970-5_30.

Kshetri, Tek (Sept. 2018). "NDVI, NDBI & NDWI Calculation Using Landsat 7, 8". In.

MacQueen, James et al. (1967). "Some methods for classification and analysis of multivariate observations". In: *Proceedings of the fifth Berkeley symposium on mathematical statistics and probability*. Vol. 1. 14. Oakland, CA, USA, pp. 281–297.

OpenStreetMap contributors (2024). *Planet dump retrieved from https://planet.osm.org*. https://www.openstreetmap.org.

Soralump, Suttisak et al. (2021). "Assessment of landslide behaviour in colluvium deposit at Doi Chang, Thailand". In: *Scientific Reports* 11. URL: https://api.semanticscholar.org/CorpusID:244661513.

Steinhaus, Hugo et al. (1956). "Sur la division des corps matériels en parties". In: *Bull. Acad. Polon. Sci* 1.804, p. 801.

Tadono, T. et al. (2016). "GENERATION OF THE 30 M-MESH GLOBAL DIGITAL SURFACE MODEL BY ALOS PRISM". In: *The International Archives of the Photogrammetry, Remote Sensing and Spatial Information Sciences* XLI-B4, pp. 157–162. DOI: 10.5194/isprs-archives-XLI-B4-157-2016. URL: https://isprs-archives.copernicus.org/articles/XLI-B4/157/2016/.

Yalcin, Ali (2007). "The effects of clay on landslides: A case study". In: *Applied Clay Science* 38.1-2, pp. 77–85.

Reflections on Learning Process

I felt that leaving the support of the highly structured workshops was quite a welcome change. I found it significantly more difficult to follow instructions exactly than find my own way through tasks. Maybe it would be good to have some kind of voluntary exercises to do between labs (without direct support) so we could learn to do stuff a bit more independently. The current workshops did serve as an excellent guide on how to perform certain techniques though. Overall, I've really enjoyed learning the module.

Acknowledgements

Map data copyrighted OpenStreetMap contributors and available from https://www.openstreetmap.org Landsat-8 image courtesy of the U.S. Geological Survey Precipitation data used in this report came from WorldClim Elevation data used in this report have been provided by the Japan Aerospace Exploration Agency (JAXA).

Appendix

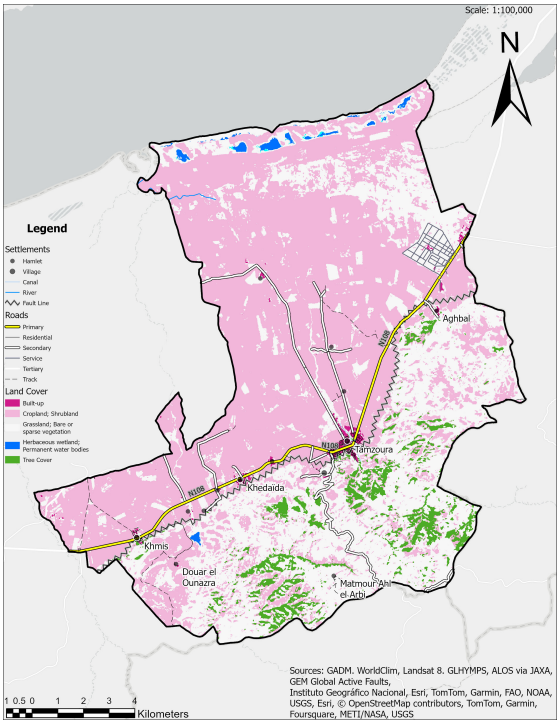

Figure 7: Layer showing the slope data across Tamzoura, divided cleanly by the fault line.

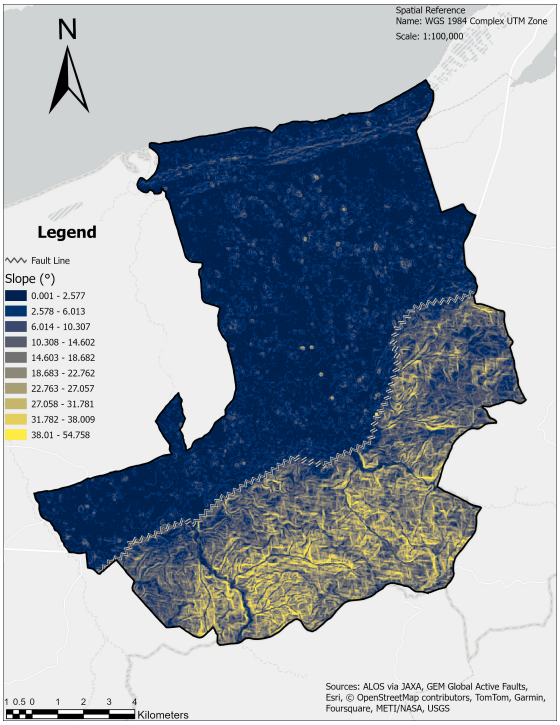

Figure 9: Layer showing the slope data across Tamzoura, divided cleanly by the fault line.

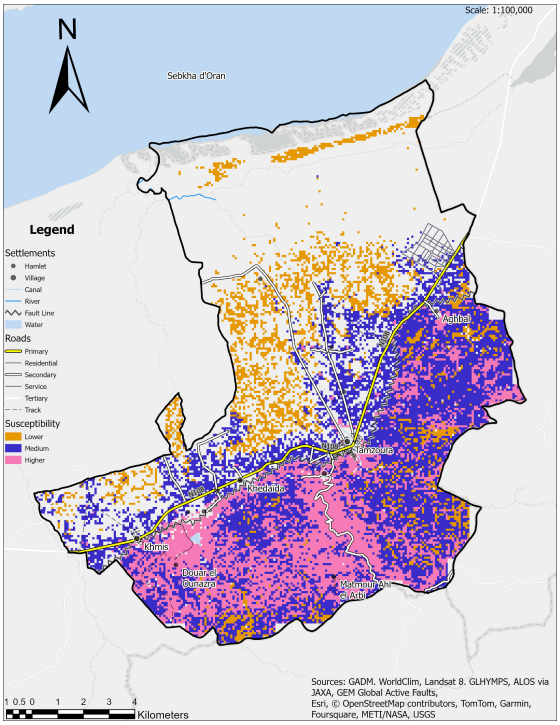

Figure 8: All Effects full Susceptibility Map

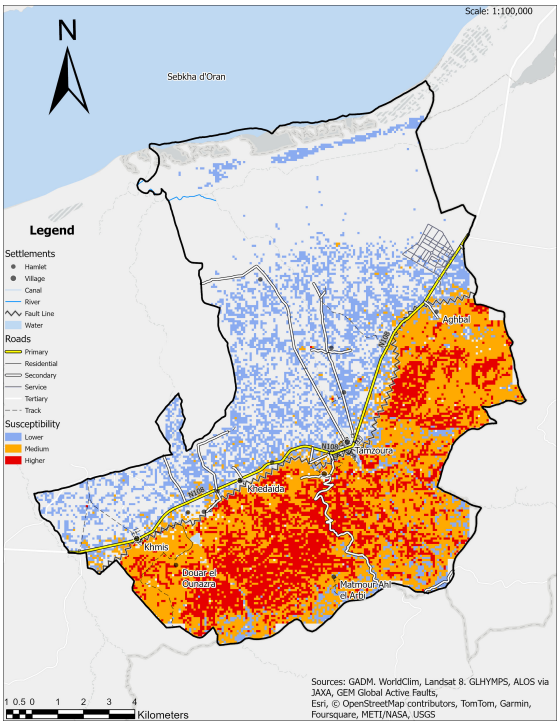

Figure 10: Main Effects full Susceptibility Map